



Large-Scale Instrumented Triaxial Setup for Investigating the Response of Soft Clay Reinforced with Sand Column Groups

Abdurrahman Almikati, S.M.ASCE¹; Shadi Najjar, A.M.ASCE²; and Salah Sadek, M.ASCE³

Abstract: Granular columns are widely used as a soil improvement solution adopted in the case of soft clays in an effort to increase their bearing capacity and stiffness. Granular columns, whether sand drains or gravel columns, are designed and constructed in groups and not as individual elements, given that there is a clear need to study the group effects and load sharing under various drainage conditions. Toward this need, a new fully instrumented triaxial test setup was developed and utilized to investigate the overall response of the composite. Particular emphasis was placed on monitoring pore-water pressures and contact stresses over the sand columns and the surrounding clay. The results from clay specimens that were reinforced at area replacement ratios of 17.1% and 30.4% indicate that the test setup is capable of quantifying the distribution of the stresses in the columns and the surrounding clay at different levels of axial strain. As such, previous information about the dependency of the stress concentration ratio on the area replacement ratio, axial strain, rate of loading, and drainage conditions could be inferred. It is anticipated that the insights gained and reported in this paper will facilitate the development of design methodologies for soft clays reinforced with sand column groups. **DOI: 10.1061/(ASCE)GM.1943-5622.0002148.** © 2021 American Society of Civil Engineers.

Author keywords: Triaxial testing; Reinforced Soft clays; Group sand columns; Contact stresses; Stress concentration ratio; Instrumentation and measurement.

Introduction and Background

The use of granular inclusions in the form of sand drains or gravel (stone) columns is a common ground improvement solution in many geotechnical engineering applications, particularly those involving relatively light to moderately loaded systems extending over large areas (Najjar et al. 2010). This ground modification technique consists primarily of replacing a certain area of weak soft clay with stiff granular columns. The area replacement ratio could range anywhere between 5% and 40%, with optimum replacement ratios mostly in the range of 30%–40%, above which the interaction between the soil matrix and the granular columns may become inefficient (Black et al. 2011).

Granular columns are designed and constructed in groups rather than as individual elements, given that there is a clear need to study the group effects and load sharing under various drainage conditions. Most of the studies reported in the literature focused on the response of soft clays reinforced with a *single* granular column. Experimental investigations were predominantly based on tests conducted in large one-dimensional (1D) loading chambers (Stuedlein and Holtz 2012; Najjar 2013). Such testing arrangements may be considered to be nonrepresentative of actual field

conditions. This is true due to the inability to control the drainage conditions and rate of loading to mimic the field loading, in addition to the inability to model the correct field stress state, which differs significantly from the stress levels encountered in such model experiments. As a result, findings from laboratory scale model tests, even if conducted on specimens reinforced with column groups, cannot be generalized or extrapolated to the field scale.

In order to overcome these limitations, significant interest was shown by researchers to use a triaxial testing setup to investigate the response of specimens that are reinforced with sand (or stone) columns while controlling the stress state, the global drainage conditions, and the loading rate. Triaxial testing conditions allow for the control of (1) drainage during testing (drained, undrained, or partially drained) and (2) confining stresses that could be selected to be in the same order of magnitude as those expected in the field. Many researchers studied the behavior of granular columns installed in soft clays in triaxial testing setups. These include the work of Juran and Guermazi (1988), Sivakumar et al. (2003), Black et al. (2006), Black et al. (2007), Kim and Kim (2007), Andreou et al. (2008), Najjar et al. (2010), Black et al. (2011), Sivakumar et al. (2011), and AlMikati et al. (2020). The vast majority of the aforementioned triaxial studies involve soft clays that are reinforced with a single central granular column rather than column groups.

The existing works available in the literature that specifically addressed column groups include the efforts of Hugher and Withers (1974), Bachus and Barksdale (1984), Wood et al. (2000), Black et al. (2006, 2007), White et al. (2007), Murugesan and Rajagopal (2010), Fattah et al. (2011), Miranda et al. (2017), and Aslani et al. (2019). The majority of these studies utilized large 1D loading chambers to investigate the effects of (1) spacing between adjacent columns; (2) configuration of columns in the group; (3) column diameter and penetration depth; and (4) area replacement ratio on the response of the composite.

The measurement of contact stresses on granular columns and the surrounding clay annulus has been identified as a key element in understanding the stress transfer mechanism between the granular

¹Ph.D. Student, Dept. of Civil and Environmental Engineering, American Univ. of Beirut, Bliss St., Beirut 1107 2020, Lebanon (corresponding author). ORCID: <https://orcid.org/0000-0001-9686-6244>. Email: aam65@mail.aub.edu

²Associate Professor of Civil and Environmental Engineering, American Univ. of Beirut, Bliss St., Beirut 1107 2020, Lebanon. ORCID: <https://orcid.org/0000-0003-1824-4540>. Email: sn06@aub.edu.lb

³Professor of Civil and Environmental Engineering, American Univ. of Beirut, Bliss St., Beirut 1107 2020, Lebanon. ORCID: <https://orcid.org/0000-0002-0672-8305>. Email: salah@aub.edu.lb

Note. This manuscript was submitted on October 14, 2020; approved on May 17, 2021; published online on July 28, 2021. Discussion period open until December 28, 2021; separate discussions must be submitted for individual papers. This paper is part of the *International Journal of Geomechanics*, © ASCE, ISSN 1532-3641.

inclusions and the surrounding matrix (Aslani et al. 2019). Contact stress measurements at different stages of loading allow for determining the stress concentration ratio, which is defined as the ratio of the stress in the granular column to the stress in the clay. This ratio is a key parameter when designing reinforced soft clay systems. Several parameters and factors affect the magnitude of the stress concentration ratio and these are: the relative stiffness of the column and clay material, drainage conditions, slenderness of the column, area replacement ratio, and other construction details (Hu 1995).

Table 1 summarizes results from all published studies that targeted the measurement of the stress concentration ratio in a laboratory setting (Charles and Watts 1983; Bachus and Barksdale 1984; Juran and Guermazi 1988; Wood et al. 2000; McKelvey et al. 2004; Murugesan and Rajagopal 2010; Cimentada et al. 2011; Fattah et al. 2011; Ghazavi and Afshar 2013; Miranda et al. 2017; McCabe and Killeen 2017; Nazariafshar et al. 2019). In these studies, continuous measurement of the contact stresses on the column and clay using miniature pressure sensors and load cells allowed for the investigation of the buildup of stress concentration in the granular column with axial strain. The tests in Table 1 are limited to loading setups involving axial compression, including triaxial compression, footing loading, and area loading.

Information in Table 1 indicates that 10 out of the 11 reported studies utilized laboratory-scale 1D model setups or large-scale odometers as a basis for testing. As indicated in Table 1, the only triaxial-based study that measured the stress concentration factor utilized a single column rather than column groups. Finally, the results in Table 1 show that the vast majority of the studies did not quantify the effect of the drainage conditions and rate of loading on the reported stress concentration factors. As such, there appears to be a clear need for additional studies that are aimed at measuring stress concentration factors within triaxial settings for soft clays that are reinforced with column groups under contrasting drainage conditions. The objective of this study is to address the aforementioned need.

To achieve this objective, a newly developed, fully instrumented large-scale triaxial test setup is utilized to investigate the overall response of the composite with particular emphasis on monitoring pore-water pressure and contact stresses over sand columns and the surrounding clay. The metrics for assessing the success in achieving this objective are based on showing that the proposed test setup is capable of quantifying the distribution of the stresses

between the sand columns and the surrounding clay at different levels of axial strain while controlling drainage and enforcing confining stress levels that are consistent with field applications. A major constraint in designing the test setup was the need to test soft clay specimens that are reinforced with column groups rather than a single column. This constraint necessitated the utilization of a triaxial setup capable of accommodating large-diameter cylindrical matrix samples. Details about the novel test setup, including the design of the cap, sensors, instrumentation, and data acquisition are presented in the following section.

It should be noted that the large-scale reinforced specimen that was used in this study extends the unit cell triaxial model to a more realistic group model that could reflect the interaction among the different columns in the group. The triaxial boundary conditions in the case of the group do not diverge from the triaxial boundary conditions of the unit cell in Najjar et al. (2010, 2020), since the reinforced clay specimen in both cases is confined by a constant confining pressure (σ_3) and is allowed to bulge in the radial direction during triaxial compression. The benefit of large cell tests with groups is that they allow for multiple arrangements of columns at various replacement ratios while modeling the interaction between the columns in the group and the surrounding clay. The normalized spacing between the sand columns (s/d) and their location within the specimen were carefully chosen so that the reinforced specimen will represent the area replacement ratio and the s/d ratio of a subset of a large group in the field. It is anticipated that the setup and results presented herein will facilitate the development of design methodologies of clays reinforced with column groups.

Triaxial Test Setup and Instrumentation

A Humboldt triaxial cell capable of testing cylindrical specimens with a diameter of 145 mm and a height of 300 mm was customized [Fig. 1(a)] to allow for the collection of data from: three miniature contact pressure sensors, three pore pressure sensors, a volume change apparatus with a linear variable differential transformer (LVDT), a load cell, and a displacement sensor (LVDT). The setup was designed to allow for testing soft kaolinite clay specimens that were reinforced with up to four sand columns arranged in a square configuration, as indicated in Fig. 1(b).

Table 1. Experimental research programs with stress concentration factors reported

Reference	Type of experiment (S = single, G = group)	Loading conditions (stress = stress controlled strain = strain controlled D = drained, U = undrained)	Area replacement ratio (%)	Sensor used for stress measurement (LC = load cell, PS = pressure sensor) m = miniature	Stress concentration factor, n (U = undrained, D = drained F = fully pen., P = partial pen.)
Charles and Watts (1983)	1-g Cons. ^a (S)	Stress (D)	21, 33	m-PS	$a_r = 33\%$, $n = 4.8$ $a_r = 21\%$, $n = 2.2$
Bachus and Barksdale (1984)	1-g (S/G)	Stress (D) Strain (D)	7, 25	LC	S— $n = 2.8$ – 4.2 G— $n = 2.5$ – 4.0
Juran and Guermazi (1988)	TX (S)	Strain (D/U)	4	LC	$n_D = 6.0$, $n_U = 3.0$
Wood et al. (2000)	1-g (G)	Strain (D)	10, 30	m-PS	$n_P = 6$
McKelvey et al. (2004)	1-g (G)	Strain (U)	24	m-PS	$n_F = 5.2$, $n_P = 2.8$
Murugesan and Rajagopal (2010)	1-g (G)	Stress (D)	23	PS	$n = 7.0$ – 9.0
Cimentada et al. (2011)	1-D Cons. ^a (S)	Stress (D)	6.25, 11	m-PS	$n = 2.5$ – 9.0
Fattah et al. (2011)	1-g (S/G)	Stress (U)	5, 20	LC	$n = 1.4$ – 6.0
Ghazavi and Afshar (2013)	1-g (S/G)	Strain (D)	16	m-LC	$n = 5.5$ – 6.2
Miranda et al. (2017)	1-g Cons. ^a (S)	Stress (D)	11	m-PS	$n = 3.0$ – 6.0
Nazariafshar et al. (2019)	1-g (G)	Strain (U)	19	m-PS	$n = 2.2$ – 4.3

^aLarge-scale odometer.

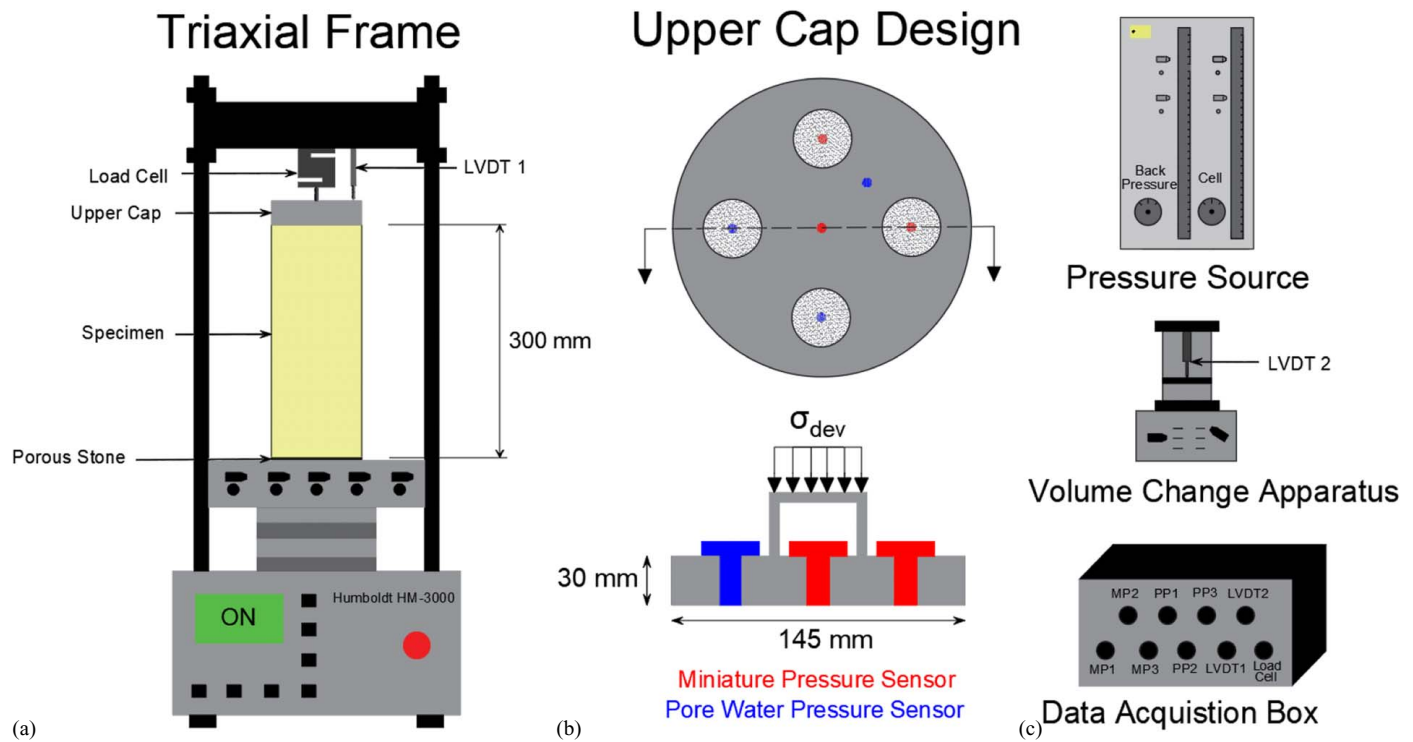


Fig. 1. Testing setup showing: (a) an upper cap design with dimensions; (b) a testing frame with sample dimensions; and (c) a data acquisition box, pressurized water source, and the volume change apparatus.

Upper Cap Design

An upper cap with a diameter of 145 mm was designed and fabricated from a solid aluminum block to include housings for three access ports for water sources in addition to housings for three miniature contact pressure sensors [Fig. 2(a)]. Porous stones were fitted into the housings of the pore-water ports and they were maintained flush with the bottom side of the cap. Similarly, the active part of the pressure sensor [Fig. 2(b)] was maintained flush with the bottom side of the upper cap.

Two miniature pressure sensors (MP1 and MP2) and two pore-water ports (WS and PP3) are arranged in a square configuration 44 mm away from the center of the cap, with a third miniature pressure sensor (MP3) located at the upper cap's center. The third pore-water port in the upper cap (PP2) is located between MP1 and MP2 in order to allow for the measurement of the pore pressure in the clay matrix between two sand columns. The pore-water port (WS) allows for the application of backpressure from the top side of the specimen in addition to the measurement of volume change in the consolidation and drained shearing stages. Although most of, if not all, the sensors are installed within the upper cap, an additional pore-water pressure sensor (PP1) is connected to one of the tubes that accesses the lower porous stone at the base of the specimen.

A three-dimensional side view of the upper cap (Fig. 3) shows the complete assembly of the upper cap with sensors, fittings, and tubing. The miniature pressure sensors' electronic board is close to the active part of the sensor [Fig. 2(b)], which prohibits installing the sensor without proper isolation of the electronic board from the sensor itself. As such, it was critical to ensure complete water tightness of the fittings to eliminate the possibility of cell water leakage into the sensor chambers through any of the tubing and connections.

Pressure Control and Volume Measurements

As shown in Fig. 1(c), two water pressure lines control the stress state in the triaxial cell. The first is a pore-water line that is connected to a volume change device that allows for the measurement of volumetric change during the different testing stages. The second is a cell pressure line that is directly connected to water in the triaxial chamber to control the isotropic confining pressure around the specimen. The volume change apparatus has a double-acting piston for measuring volume change during consolidation or drained shear with a capacity of 100 mL. It is equipped with a displacement transducer that is calibrated to measure the volume of water passing through the chamber. A T-connection is used to connect the volume change device to the appropriate pore-water ports in the upper and lower caps in contact with the soil specimen, thus allowing for the application of a controlled backpressure to both ends of the specimen. The back pressure and the cell pressure are controlled from a panel that is pressurized using compressed air.

The Humboldt HM-3000 master loader and frame was used to run the triaxial tests. It is capable of loading large soil specimens up to 145 mm in diameter and 300 mm in height. The allowable shearing rates range between 0.1 and 75 mm/min. The cell chamber can withstand pressures up to 1,200 kPa.

Sensors, Data Acquisition, and Calibration

The miniature pressure sensors used in the setup are manufactured by OMEGA Engineering Company and have a capacity of 1,400 kPa [Fig. 2(b)]. The transducer diaphragm and sidewalls are made of stainless steel. The main application for these sensors is to detect and measure pressures from fluids. Their intended use in the testing setup described is to measure contact pressures above

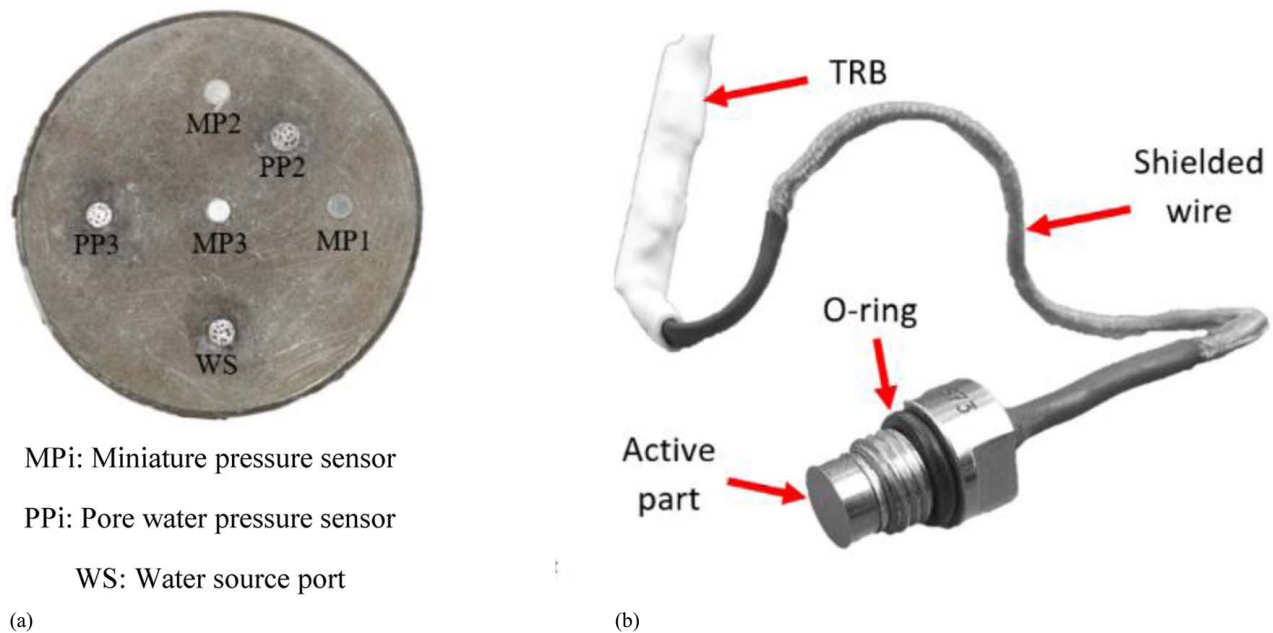


Fig. 2. Upper cap setup showing: (a) a bottom view of the top cap with miniature pressure sensors and porous stones; and (b) an omega miniature pressure sensor used.



Fig. 3. Side view of the upper cap showing the fittings and tubing to completely isolate the cell pressurized water from leaking toward the sensors and the specimens.

the clay matrix and above the sand-reinforcing column. In order to test their ability to provide reliable measurements of contact stresses with soils (kaolinite clay and sand), the sensors were calibrated under three conditions: (1) contact with water; (2) contact with kaolin clay; and (3) contact with sand. Under conditions of water contact and kaolin clay contact, the sensors exhibited a linear response and showed repeatable calibration coefficients. This was somewhat expected given the clay's very small particle size, plasticity, and saturation, where minimal variations and noises were detected in the measurement of contact stresses above the clay matrix.

Conversely, the calibration of the sensors using the dry Ottawa sand yielded nonlinear results. This was attributed to large contact forces between the sand grains, which are larger than the clay

particles, and the sensor's membrane. Further calibration using saturated sand interface resulted in a more-or-less linear response in the pressure range of interest. Since all specimens in the test program were back-pressure-saturated prior to shearing, it was considered that the pressure sensors would yield reliable measurements for both the sand and the clay in the large-scale composite specimens, provided the respective calibration constants were applied.

It should be noted that calibration using pressurized water was done using an enclosed triaxial chamber, with the pressure sensors mounted flush with the bottom side of the loading cap. The calibration of the sensors using kaolin clay or sand was done using a custom-made 1D odometer consolidation upper cap that has a central manufactured space for the pressure sensors to be mounted in. The 1D setup has a closed-loop pressure option that helps maintain a uniform applied pressure.

The electric signals from the pressure sensors exhibited some noise due to issues related to connections, wiring, and soldering. The noise in the voltage was found to be minimal during calibration in water. The voltage output from clay and sand calibrations gave linear and repetitive results. The noise was filtered using in-line amplification with a TL072CP operational amplifier from Texas Instrumentation. The TL072CP was also used to amplify the output to values in the order of 0.5–3 V that is suitable for the data acquisition module.

The pore pressure sensors did not present any problems or challenges given that the active component of the sensor is outside the triaxial setup. All tubes connected to the pore pressure sensors were maintained saturated at all times. The pore pressure sensors incorporated into the testing setup are from Ametek (Leicester, UK), with a maximum capacity of 1,400 kPa. All sensors were connected to a data acquisition box that houses the data acquisition modules, signal conditioning, signal amplification, and noise filtering. The modules used were from National Instruments and the interface adopted for data collection was LabVIEW (2017). A custom-designed graphical user interface was used to control data collection from all nine sensors and provide real-time plots of the data during the test.

Material Characterization

The materials used in this testing program were kaolin clay and Ottawa sand. Detailed properties of these materials are presented in the following sections.

Kaolin Clay

The kaolin clay (Supreme China Clay) was sourced from the United Kingdom. It had a liquid limit of 65%, plasticity index of 19%, and specific gravity of 2.56. A 1D consolidation test was conducted on a 50-mm-diameter specimen trimmed from a sample consolidated from slurry under a vertical stress of 100 kPa. Seven loading and three unloading increments were used to determine the e -log p curve, where each increment was left for 24 h to complete the primary consolidation stage. The resulting e -log p curve for the kaolin clay is presented in Fig. 4. The recompression (C_r), compression (C_c), and swelling (C_s) indices were determined to be 0.19, 0.50, and 0.17, respectively. The preconsolidation pressure was determined to be 92 kPa using the Casagrande (1936) method, indicating that the 100 kPa consolidation pressure that was applied to the slurry in the 1D consolidometers may not have fully transferred to the specimen due to frictional losses along the mold surfaces.

In order to characterize the shear strength of the kaolin clay, three isotropically consolidated undrained (CU) tests and three consolidated drained (CD) tests were conducted on back-pressure-

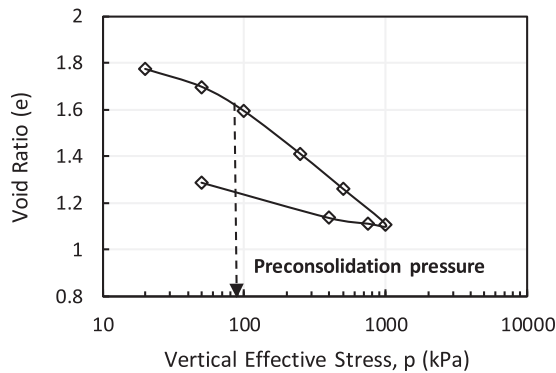


Fig. 4. e -log p for normally consolidated kaolin clay.

saturated specimens with a height of 142 mm and a diameter of 71 mm at effective confining pressures of 100, 150, and 200 kPa. The results of the drained and undrained triaxial tests on kaolin clay are presented in Figs. 5 (a and c), respectively.

The stress–strain response from the consolidated drained tests [Fig. 5(a)] indicated a strain-hardening effect for all confining pressures up to an axial strain of 16%, where a peak deviatoric stress was reached. The volumetric change indicated contractive behavior that is typical of soft and normally consolidated clay specimens that are sheared in a drained condition toward the critical state. The effective drained Mohr–Coulomb failure envelope was used to determine the drained shear strength parameters of the kaolin clay. The measured effective strength parameters for kaolin clay were $c' = 0$ kPa and $\phi' = 21.8^\circ$.

For the consolidated undrained tests, the variation in the deviatoric stress and the excess pore-water pressure with axial strain [Fig. 5(c)] indicates that the kaolin clay used in this experimental program softens at axial strains in the order of 10%–12%. The maximum deviatoric stresses were 56.9, 79.4, and 100.4 kPa corresponding to $s_u/(\sigma'_3)_0$ ratios of 0.28, 0.26, and 0.25 respectively, where s_u represents the undrained shear strength and $(\sigma'_3)_0$ represents the initial effective confining pressure. These $s_u/(\sigma'_3)_0$ ratios are typical of normally consolidated clays sheared in undrained conditions (Lin and Penumadu 2005). For the different effective confining pressures of 100, 150, and 200 kPa, the maximum recorded pore-water pressures were 60.0, 92.9, and 119.3 kPa, corresponding to Skempton pore pressure parameters A_f of 1.06, 1.13, and 1.19, respectively (Skempton 1954).

Table 2. Physical and mechanical properties of Ottawa sand

Soil property	Value
D_{10} (mm)	0.22
D_{30} (mm)	0.3
D_{60} (mm)	0.5
Specific gravity	2.65
Coefficient of uniformity (D_{60}/D_{10})	2.3
Coefficient of curvature ($D_{30}^2/(D_{60} \times D_{10})$)	0.82
Maximum void ratio; e_{max}	0.75
Minimum void ratio; e_{min}	0.49
Angle of internal friction (ϕ) $^\circ$	39

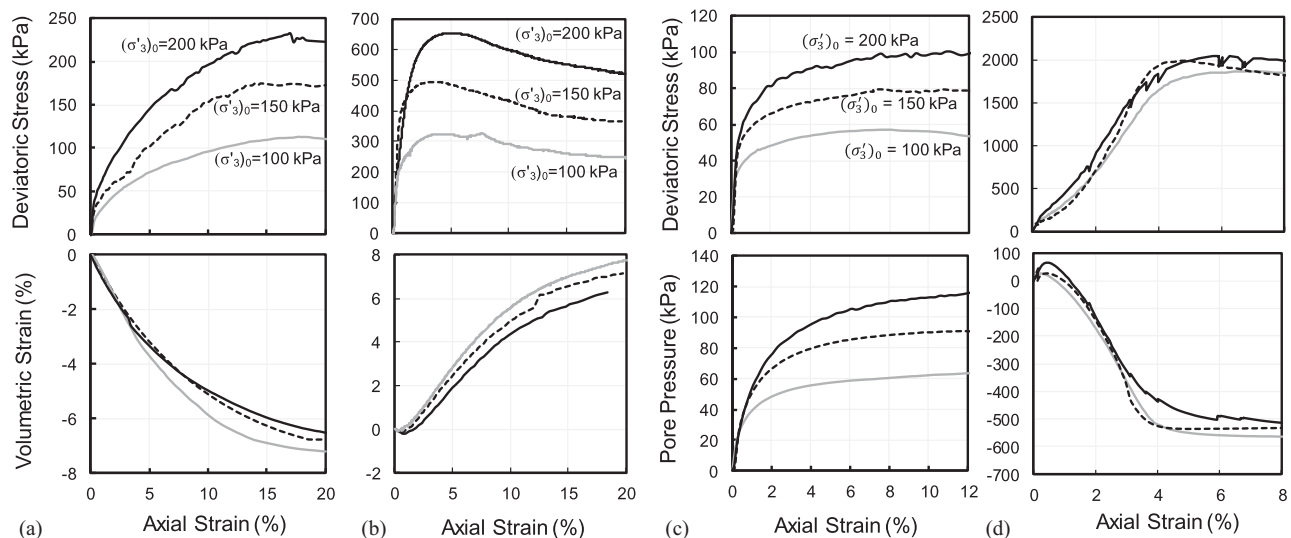


Fig. 5. Results of CD and CU triaxial tests on kaolin clay and Ottawa sand: (a) kaolin—CD; (b) sand—CD; (c) kaolin—CU; and (d) sand—CU.

Table 3. Laboratory testing program and results

Test number	Drained (<i>D</i>) or Undrained (<i>U</i>)	Diameter of sand column (mm)	Number of sand columns	Area replacement ratio A_c/A_s (%)	Maximum deviatoric stress (kPa)	Excess pore pressure (kPa)	Volumetric strain (%)	Increase in deviatoric stress (%)	Reduction in excess pore pressure (%)	Reduction in volumetric strain (%)
1	U	0	0	0	56.6	61	—	0.00	0.00	—
2	U	30	4	17.1	78.3	45	—	38.4	26.2	—
3	U	40	4	30.4	146.5	12	—	158.8	80.3	—
4	D	0	0	0	119.0	—	6.44	0.00	—	0.00
5	D	30	4	17.1	128.1	—	4.57	7.65	—	29.0
6	D	40	4	30.4	166.4	—	0.97	40.0	—	84.9

Ottawa Sand

The sand used in the test program is classified as poorly graded Ottawa sand (SP) according to the Unified Soil Classification System. The physical and mechanical properties of the sand are presented in Table 2. The sand shear strength was determined using isotropically consolidated drained and undrained triaxial tests that were conducted on specimens with a height of 142 mm and a diameter of 71 mm at initial confining pressures of 100, 150, and 200 kPa. The specimens were prepared at a dry density of 1.74 Mg/m^3 corresponding to a relative density of 85%, and a void ratio of 0.53. All sand columns used in the testing program had a density of $1.74 \pm 0.01 \text{ Mg/m}^3$ ensuring high consistency during testing.

The drained triaxial test results presented in Fig. 5(b) show stress–strain and volumetric responses that are typical of dense sand. Clear peaks were exhibited in the stress–strain responses at axial strains in the order of 3%–5%, followed by softening all the way to the critical state. The softening was associated with the dilation of the dense sand during drained shear. The drained tests indicated that the sand can be characterized with a $c' = 0 \text{ kPa}$ and $\varphi' = 39.0^\circ$. The consolidated undrained test results in Fig. 5(d) reflect the dilatative tendency of the dense sand through the generation of large negative excess pore-water pressures during undrained shearing.

Laboratory Testing Program

The testing program is summarized in Table 3. In total, three isotropically consolidated drained (CD) and three isotropically consolidated undrained (CU) triaxial tests were performed on specimens having a diameter of 145 mm and a length of 295 mm. Tests were performed on control specimens and specimens reinforced with a group of four nonencased, fully penetrating dense sand columns with diameters of 30 and 40 mm, representing area replacement ratios of $a_r = 17.1\%$ and 30.4% , respectively. The columns were installed in predrilled holes using a square arrangement at 44 mm offset from the specimen center. The holes were drilled using a custom-fabricated augering apparatus. All specimens were saturated using a back pressure of 300 kPa and isotropically consolidated under an effective confining pressure of 100 kPa. Skempton B values were around 0.98 for all tests (Skempton 1954), indicating adequate degrees of saturation. All tests were strain controlled and terminated at axial strains of $\sim 20\%$. The strain rate chosen for every test was a function of t_{50} as per the ASTM (2011) standards.

Clay Specimen Preparation

Kaolin clay (China Clay) powder was mixed with water at two times its liquid limit (i.e., 130% water content) to form a slurry. The mixture was then poured into custom-fabricated split PVC



Fig. 6. Custom-fabricated 1D consolidometers.

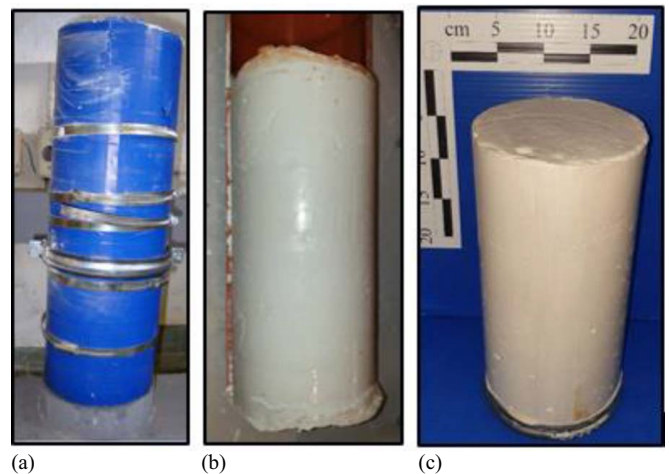


Fig. 7. (a) Sealed PVC split sections; (b) dismantling of PVC sections; and (c) kaolin specimen consolidated to 100 kPa.

pipes and subjected to 1D consolidation using a sequenced application of dead weights. Three 1D consolidometers were fabricated for this purpose (Fig. 6). Custom-fabricated split PVC pipes functioned as split molds 3 mm thick, 500 mm high, with an internal diameter of 145 mm. The slurry was placed inside the well-tightened PVC pipe segments [Fig. 7(a)]. High-strength duct tape and metallic bands were used to confine the split PVC while maintaining

negligible lateral strains during 1D consolidation of the slurry under a vertical applied pressure of up to 100 kPa.

The advantage of using split molds is that an undisturbed, relatively soft, homogenous clay specimen could be retrieved (Fig. 7) with minimal disturbance. Perforated metallic upper and lower caps with filter paper served as porous boundaries. Dead weights were seated on a circular steel plate that transferred the load to the top of the clay through a cylindrical steel rod. Dead weights were added gradually and in increments based on the time schedule presented in Table 4. The loading schedule was selected using the trial and error method to achieve repeatable and uniform samples with minimal disturbance. The quality of the specimens thus formed was evident in (1) the uniformity in the final specimen height (~ 315 mm) and (2) consistency in the water content along the specimen length. This consistency was tested through a trial

Table 4. Loading sequence during 1D consolidation

Test information	S1	S2	S3	S4	S5	S6	S7
Applied weight (kg)	0	10	20	40	80	120	170
Applied pressure (kPa)	0	6	12	24	48	71	101
Duration (h)	12	24	24	24	24	24	24

Note: S1 = Stage No. 1 and so on.

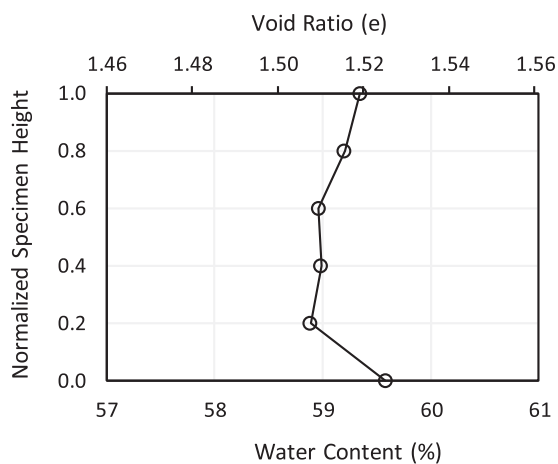


Fig. 8. Variation in water content and void ratio along the height of the sample after 1D consolidation.

experiment in which a specimen was sliced into six pieces and the water content and void ratio were determined for each slice. The variation in the water content and void ratio along the height of the specimen, as presented in Fig. 8, indicates a relatively uniform degree of consolidation along the specimen height.

All samples were subsequently isotropically reconsolidated at 100 kPa in the triaxial cell, which eliminated any 1D stress history that might have existed in the sample following consolidation in the 1D consolidometers.

Construction of Sand Columns

After dismantling the cylindrical kaolin specimen from the PVC consolidometers and trimming it to the specified final height of 295 mm, the sample was placed in a custom-fabricated augering apparatus that is capable of drilling up to 300 mm inside the soil specimen (Fig. 9). Two auger bits were then used to drill either 30 mm or 40 mm diameter holes in the clay specimen to form the column group. Preprepared frozen sand columns were then placed in their respective predrilled holes. The sand columns were frozen in prefabricated 3D-printed tubes. The tubes were printed as split molds with a total height of 300 mm and a wall thickness of 2 mm. The freezing method was used for the preparation of sand columns (Sivakumar et al. 2004; Black et al. 2007) as it has shown good repeatability and consistency in terms of the relative density of the sand columns (Najjar et al. 2010).

The sand split tubes were held in place using a high-strength duct tape to ensure no lateral strains during sand freezing. The sand was filled in layers while vibrating the tubes from the outside to achieve a final dry density of 1.74 ± 0.01 Mg/m³, corresponding to 85% relative density. Following densification, water was added to achieve a water content of around 20%. The columns were then placed in the freezer for at least 24 h. After drilling each hole, a sand column was removed from the freezer, the tubes split, and the column inserted into the drilled hole and allowed to thaw (Fig. 9).

Test Results and Analysis

The modified triaxial test setup with its newly devised instrumentation was used to run large-scale drained and undrained triaxial tests on control clay specimens and specimens that were reinforced with a group of four sand columns distributed in a square arrangement. All samples were isotropically consolidated under an



Fig. 9. Drilling holes in kaolin specimen and sand column installation.

effective confining pressure of 100 kPa prior to the shearing stage, after ensuring saturation through applying an incremental back-pressure of 300 kPa. The test results are presented in Table 1 and include two tests on control clay specimens, two tests on specimens reinforced with an area replacement ratio $a_r = 17.1\%$, and two tests on specimens reinforced with an area replacement ratio $a_r = 30.4\%$. The analysis focused on the effect of sand columns on: (1) consolidation; (2) bearing capacity and stress distribution; (3) reduction in volumetric strain and pore pressure during shearing; and (4) development of stress concentration within the sand columns.

The drained and undrained triaxial tests were conducted in accordance with ASTM standards. In the consolidated drained tests, the rate of shearing was calculated as $\dot{\epsilon} = \epsilon_f / 120t_{50}$, where ϵ_f = axial strain at failure (chosen as 10%) and t_{50} = time corresponding to a degree of consolidation of 50%. For the consolidated undrained tests, the rate of shearing was calculated as $\dot{\epsilon} = \epsilon_f / 10t_{50}$ to achieve equalization of pore-water pressure throughout the height of the specimens. As a result, the strain rate that was adopted in the consolidated drained tests ranged from 0.1 to 1.2 mm/h, while the rate adopted for the undrained tests ranged from 1.1 to 28.5 mm/h. It should be noted that in the drained tests, fully drained conditions during shearing were confirmed by monitoring the excess pore-water pressure at three locations (Fig. 1). The excess pore pressures were always in the range of $-2 \text{ kPa} \leq u_p \leq +2 \text{ kPa}$, indicating complete dissipation of excess pore-water pressure in the specimens.

Consolidation Stage

The isotropic consolidation response of the six test specimens under an effective confining pressure of 100 kPa is presented in Fig. 10. Three observations can be made from the volumetric strain versus time curves: (1) the incorporation of sand column groups in the reinforced clay specimen reduced the volumetric strain of the control specimen by about 35% and 46%, with a higher percent reduction for the higher area replacement ratio ($a_r = 30.4\%$); (2) the time required for consolidation to be completed decreased significantly as the area replacement ratio increased, with the time corresponding to 50% consolidation t_{50} decreasing from around 670 min in the case of the control clay specimen to 15 and 4 min for the specimen reinforced at $a_r = 17.1\%$ and 30.4%, respectively; and

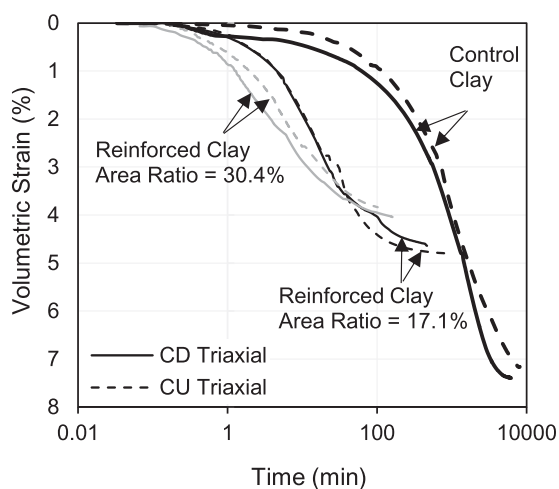


Fig. 10. Variation in volumetric strain with time during isotropic consolidation of control and reinforced specimens.

(3) the difference in the consolidation response between identical drained and undrained specimens (whether control or reinforced) was little, indicating a high level of repeatability and consistency in sample preparation, testing, and instrumentation.

The reductions observed in the volumetric strain and consolidation time are expected given the dual role that sand columns play in (1) increasing the overall stiffness of the composite specimen, and (2) enhancing radial drainage by functioning as vertical drains that reduce the horizontal drainage paths of water leaving the clay. This compares well to the findings of Baumann and Bauer (1974). In the control clay specimens, the drainage was mainly vertical with the maximum drainage distance being equal to half of the specimen height ($\sim 145 \text{ mm}$). In the reinforced specimens, the drainage direction is predominantly radial with maximum drainage distances in the order of 35 and 25 mm in the case of $a_r = 17.1\%$ and 30.4%, respectively. Since consolidation times are roughly proportional to the square of the maximum drainage distance, the reductions observed in the primary consolidation times in the reinforced specimens may be considered reasonable.

Stress–Strain Response

The stress–strain curves for the control and reinforced clay specimens are presented in Figs. 11(a and b), for the CD and CU triaxial tests, respectively. Irrespective of the drainage conditions, the results as presented in Fig. 11 indicate that the sand column group improved the bearing capacity and stiffness of the soft clay. The maximum deviatoric stress measured in the control clay specimen increased by 8% ($a_r = 17.1\%$) and 40% ($a_r = 30.4\%$) in the drained tests and by 39% ($a_r = 17.1\%$) and 159% ($a_r = 30.4\%$) in the undrained tests.

For reinforced clay specimens, the stress–strain curves in Fig. 11 show signs of strain softening starting from axial strains in the order of 5%–10%, particularly in specimens reinforced at the higher area replacement ratio of 30.4%. This response reflects the dominant role of the dense sand columns, which are expected to dilate during shear, particularly in the drained tests. The dilative tendency of the sand columns and its role in dominating the response of the composite are clearly exhibited in Fig. 11 through the variation in the volumetric strain (drained tests) and the excess pore-water pressure (in undrained tests) with axial strain. Reinforcing the clay with the sand column group reduced the compressive volumetric strain at failure in the CD tests from 6.5% to 4.6% ($a_r = 17.1\%$) and 1.0% ($a_r = 30.4\%$) and reduced the excess positive pore-water pressure in the CU tests from 60 to 45 kPa ($a_r = 17.1\%$) and 10 kPa ($a_r = 30.4\%$), respectively.

It should be noted that although the consolidated undrained tests could be considered *globally undrained*, exchange of pore water between the dilating sand columns and the surrounding compressive soft clay is inevitable. This local exchange will lead to a partial drainage of the sand columns in the group and the surrounding clay, leading to local volume change. Evidence of this partial drainage in the consolidated undrained tests is clear in the stress–strain response, which shows clear signs of strain softening. Had the sand columns been totally undrained, the generation of large negative pore pressures in the sand would have prohibited strain softening in the reinforced clay specimen.

In the consolidated undrained tests, excess pore-water pressure was measured at three locations, namely above one sand column, above the clay annulus between two sand columns, and at the bottom as a global measure for the composite soil. For all tests, the pore pressure sensors gave similar results, irrespective of their position in the specimen. This indicates that even with the relatively high rate of loading that was used in the undrained tests,

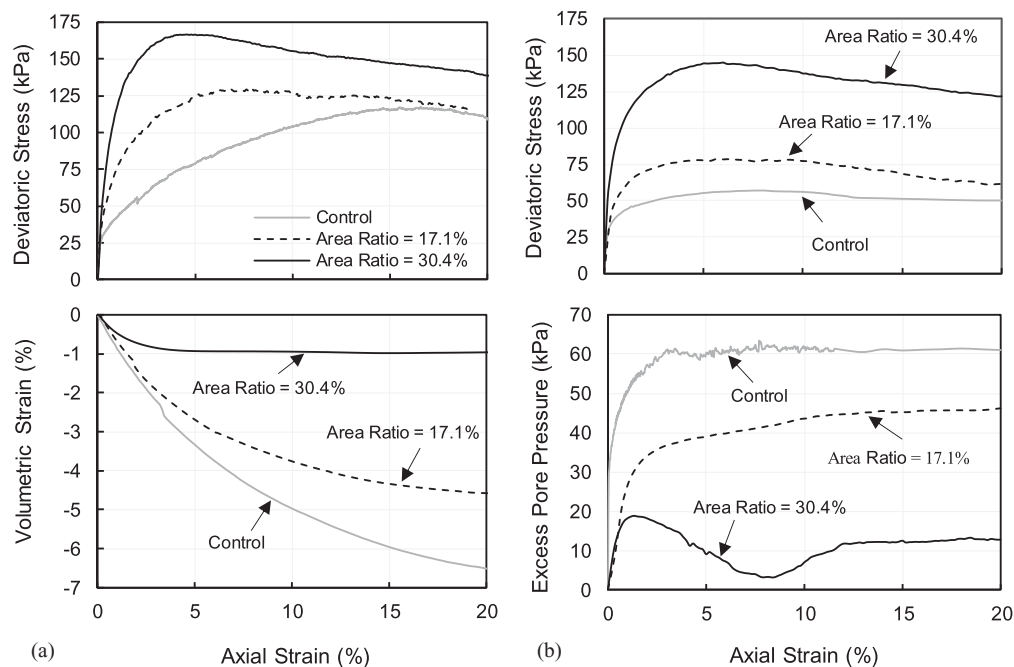


Fig. 11. Results of the large-scale triaxial tests: (a) CD; and (b) CU.

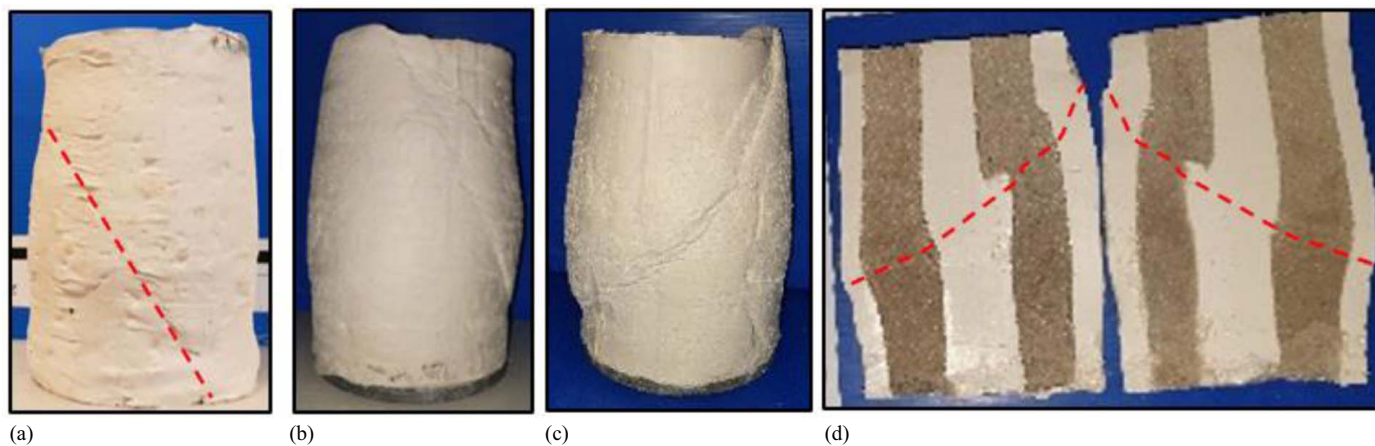


Fig. 12. External and internal mode of failure in consolidated drained triaxial tests: (a) control clay; (b) $a_r = 17.1\%$; (c) $a_r = 30.4\%$; and (d) cross section ($a_r = 30.4\%$).

equilibration of pore-water pressure occurred within the test specimen, leading to the same pore-water pressure measurement in the sand and the clay. As a result, data from only one pore-water pressure sensor are included in Fig. 11 for the undrained tests.

For the particular case of the $a_r = 30.4\%$ specimens, Fig. 11(b) clearly shows that at relatively small strains, the dilative tendency of the large diameter columns results in a significant reduction in the overall positive pore pressure generation during shearing. However, as strains accumulate toward significant values of about 10%, the gradual reduction in the pore pressure is clearly interrupted and reversed. This could be attributed to excessive shear stress/strain concentrations along the failure surface, leading to a tendency for dislocation of the sand columns and interruption of their continuity. This explanation of the observed response is supported by the pictures shown in Figs. 12(d) and 13(d), which reveal the magnitude of distortion and bulging that was induced in the sand columns at large strains.

Mode of Failure

An investigation of the mode of failure of control and reinforced clay specimens indicated that the mode of failure was affected by the drainage conditions. For the three drained tests (Fig. 12), the controlling mode of failure was uniform bulging along the height of the clay specimens. At the onset of reaching a peak in the deviatoric stress, the formation of a failure plane was observed in the control and reinforced specimens, followed by strain softening all the way to critical state conditions. On the other hand, undrained specimens (Fig. 13) that were reinforced with column groups showed localized bulging that was concentrated in the upper half of the specimens with no evidence of the formation of a failure plane (unlike the control clay undrained specimen that showed a clear failure plane).

To examine the internal mode of deformation of the sand columns in the drained and undrained tests, the specimens reinforced

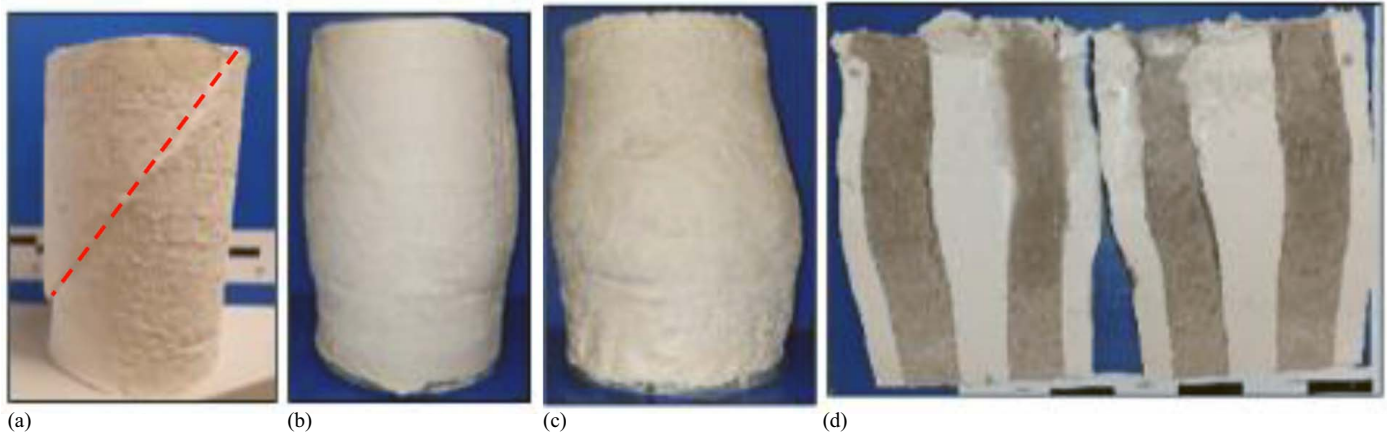


Fig. 13. External and internal mode of failure in consolidated undrained triaxial tests: (a) control clay; (b) $a_r = 17.1\%$; (c) $a_r = 30.4\%$; and (d) cross section ($a_r = 30.4\%$).

with 40 mm sand column groups ($a_r = 30.4\%$) were cut along a vertical section passing through two of the sand columns in an attempt to expose the columns and the surrounding clay. The cross sections are presented in Figs. 12(d) and 13(d) for the drained and undrained tests, respectively. For the drained test, the cross section clearly shows the failure plane cutting the sand columns along a predefined direction. No such failure plane is evident in the undrained test on the reinforced specimen. However, it is interesting to note that the sand columns in the undrained tests show asymmetrical bulging, with the columns showing signs of outward bulging toward the exterior of the specimen and almost no inward bulging toward each other. The restraining action that internal sand columns exhibit within a column group was observed in the group tests conducted by Bachus and Barksdale (1984), among others.

Measured Contact Stresses

Local contact stresses were measured using miniature pressure sensors located over two sand columns and over the clay at the center of the upper cap. The variation in the measured contact stresses with axial strain is presented in Fig. 14 for all test specimens. Also shown in Fig. 14 are the curves representing the variation of the overall global deviatoric stress with strain as measured using the global load cell.

For the control clay specimens, measuring contact stresses using the miniature pressure sensors allowed for testing the effectiveness and reliability of the miniature pressure sensors in measuring stresses under drained [Fig. 14(a)] and undrained [Fig. 14(b)] conditions. These contact stresses for the case of the control clay indicated that the three pressure sensors gave reliable and repeatable results compared with the global deviatoric stresses measured by the load cell. As expected, the stresses measured by the miniature pressure sensors at three locations exhibited some natural variability that was quantified to be within 5%–10% of the measured global deviatoric stress at least for axial strains below 10%. This observation is important since it indicates that the utilized sensors can be effectively used to monitor stresses in the drained and undrained normally consolidated kaolin clay with minimal errors.

As for the reinforced specimens, the square configuration of the four-sand column group permits stress measurement in two sand columns and in the central clay. The variations in these measured contact stresses with axial strain are presented in Figs. 14(c and d) and Figs. 14(e and f) for specimens reinforced with 30 and

40 mm sand column groups, respectively. The results from stress measurements above the sand columns (MP1 and MP2) indicated that: (1) the stiff sand columns attracted stresses that are much larger than those measured in the clay, irrespective of the drainage conditions and area replacement ratio; (2) some variability in the contact stresses is observed between the sand columns in the same composite specimen; and (3) the magnitude of the measured sand stresses in the columns is affected by the drainage conditions and the area replacement ratio.

The inherent variability in the response of identical sand columns within the same composite specimen can be attributed to multiple factors. First, slight variations in relative density between the columns in the group could affect the uniformity or the lack of the stress distribution between the columns. Second, the stresses may have been affected by slight possible rotations in the upper cap, particularly at larger strains (10%–20%) following the formation of distinct failure planes or excessive bulging. The reliability of the sensor readings can be considered as somewhat degraded by the large movements. However, all tests were continued to axial strains of 20% to get a sense of what is happening well beyond the peak response since it was assumed that even with large distortions, the measurements still give a sense of the distribution of the loads. It should be noted that the contact stresses measured by sensor MP2 in the case of the consolidated undrained test that was conducted on the sample reinforced at an area replacement ratio of 17.1% were flawed [Fig. 14(d)]. As a result, these measurements were disregarded from the analysis.

In order to validate and test the applicability and reliability of the stress measurements in the sand columns, the clay stresses that were measured by MP3 and the global deviatoric stresses for the composite clay specimen were used to back-calculate the average stress in the sand columns in the group. The variation in the back-calculated stresses in the columns with axial strain is presented in Fig. 14. The back-calculated stresses were calculated using Eq. (1) by assuming that the global deviatoric stress on the composite specimen (σ_d) was shared by the stress in the clay (σ_{clay}) and the average stress in the four sand columns (σ_{sand}) such that

$$\sigma_d A_{\text{sample}} = \sigma_{\text{clay}} A_{\text{clay}} + \sigma_{\text{sand}} A_{\text{columns}} \quad (1)$$

where A_{clay} and A_{columns} = area of the clay and the area of the sand columns in the reinforced clay specimen, while A_{sample} = total cross-sectional area of the composite specimen. Given the global

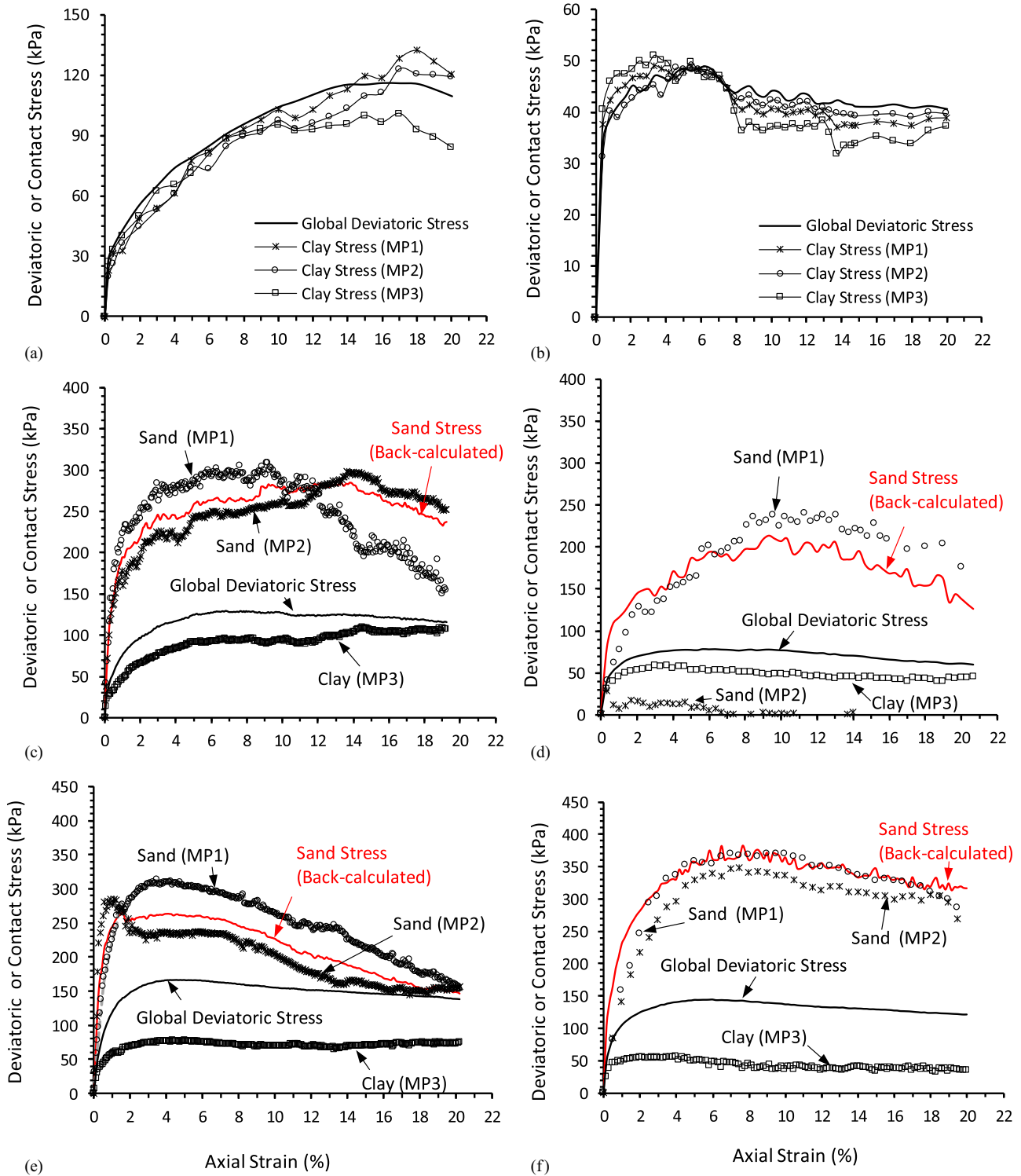


Fig. 14. Variation in deviatoric and contact stresses with strain for control and reinforced clay specimens under drained and undrained loading conditions: (a) control clay (CD); (b) control clay (CU); (c) reinforced clay ($a_r = 17\%$, CD); (d) reinforced clay ($a_r = 17\%$, CU); (e) reinforced clay ($a_r = 30.5\%$, CD); and (f) reinforced clay ($a_r = 30.5\%$, CU).

deviatoric stress (σ_d) and the measured stress (MP3) in the clay (σ_{clay}), Eq. (1) was used to back-calculate (σ_{sand}). Interestingly, the results in Fig. 14 indicate that the variation in the back-calculated average stresses in sand (σ_{sand}) with axial strain compare well with the stresses in sand measured using MP1 and MP2. In fact, the back-calculated stresses in sand constitute a realistic representation of the average stresses measured by MP1 and MP2,

irrespective of the area replacement ratio and drainage conditions. These results are important since they indicate that the stresses measured by the miniature pressure sensors are reliable and reflective of the true stress distribution in the composite specimen.

To scrutinize the mechanics of load sharing between the sand columns in the group and the surrounding clay and its dependence on the area ratio and drainage conditions, the stresses mobilized in

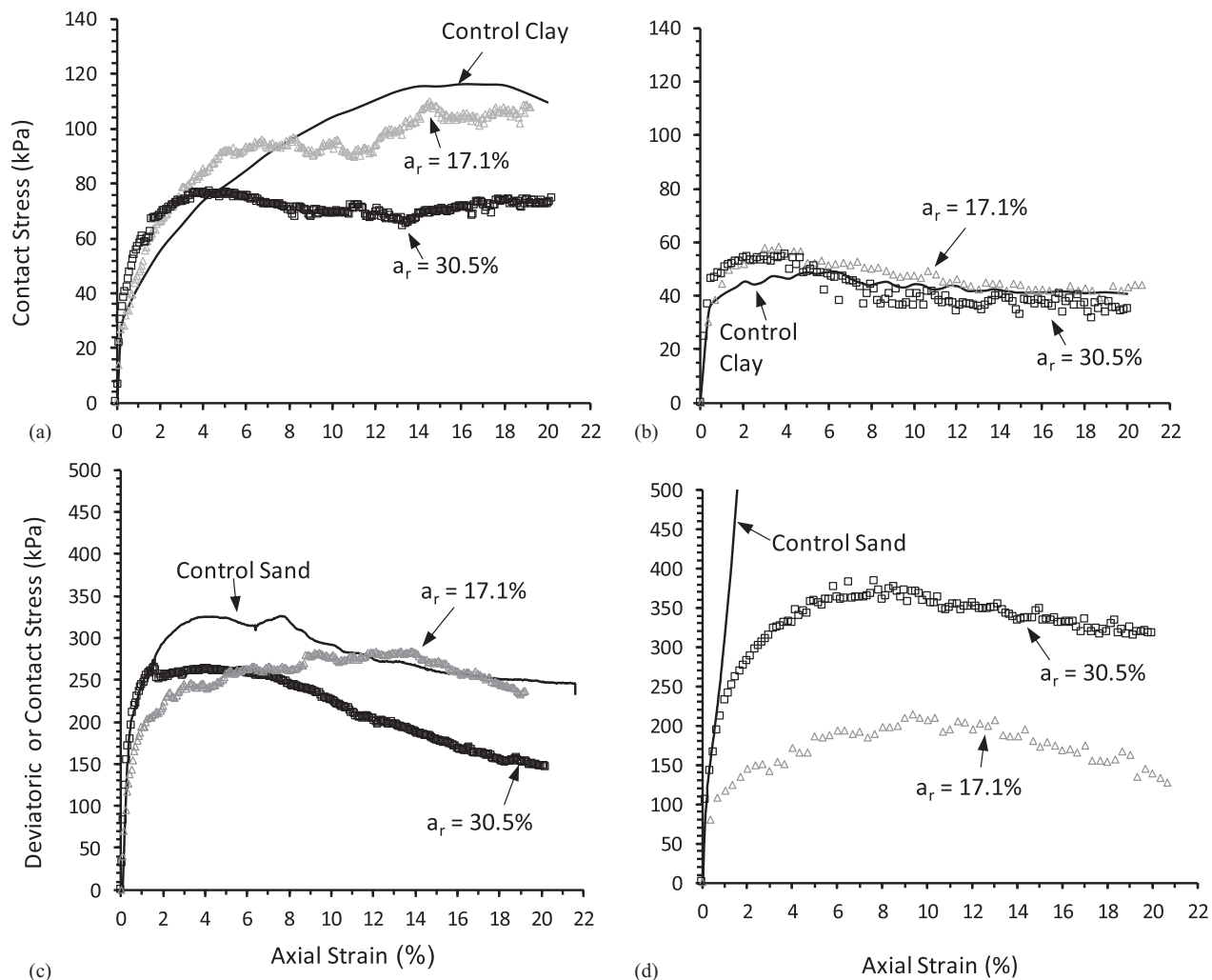


Fig. 15. Effect of area replacement ratio and drainage conditions on the mobilized clay and sand contact stresses: (a) clay stress (CD); (b) clay stress (CU); (c) sand stress (CD); and (d) sand stress (CU).

the clay (MP3) for the control and reinforced specimens were plotted on the same figures [Figs. 15(a and b) for CD and CU tests] for comparison. Similarly, the stresses mobilized in the columns in the composite specimens were compared with the deviatoric stress measured from the triaxial tests conducted on the control sand specimens [Figs. 15(c and d)].

The results presented in Fig. 15 lead to many interesting observations that show the effect of drainage conditions and area replacement ratio on the mechanics of load sharing between the sand and the clay and its dependence on the strain level. First, the results for the stresses in clay [Figs. 15(a and b)] indicate that the clay under drained conditions was able to carry higher stress than the undrained case. In fact, the stresses mobilized in the clay surrounding the columns in the drained tests approached the maximum deviatoric stress mobilized in the drained control clay specimen, without reaching it. For the case with the lower area replacement ratio ($a_r = 17.1\%$), the variation in the stress in the clay with strain was closer to the drained stress–strain response of the control clay specimen, indicating that the failure mechanism was dominated by the clay. In the composite specimen with the higher area replacement ratio ($a_r = 30.4\%$), the stresses in clay were lower, indicating that the response was governed by the stiff larger diameter sand columns.

On the other hand, the results for the undrained tests indicate that the stresses in clay in the composite specimens were (1) insensitive to the area replacement ratio and (2) consistent with the stresses measured in the control clay specimen. These observations indicate that the undrained response in the composite clay specimens was largely governed by the relatively low undrained shear strength of the clay and that the presence of sand columns did not affect the undrained shear strength of the surrounding clay. It is interesting to note that in the range of axial strain of 4%–6%, the measured stresses in clay in the composite specimens were slightly larger than those observed in the control clay specimen. This slight increase could be due to partial local radial drainage from the clay into the sand columns, leading to slight local increases in the strength of the surrounding clay, despite the fact that the tests were globally undrained.

An investigation of the gradual stress buildup in the sand columns in Figs. 15(c and d) leads to two main observations: (1) the average stresses in the sand in the column group were highly dependent on the area replacement ratio, particularly on the composite specimens that were sheared undrained; and (2) the stresses in sand mobilized in the *globally undrained* tests show clear evidence of local water exchange between the sand columns and the surrounding clay, leading to significant reductions in the mobilized stresses

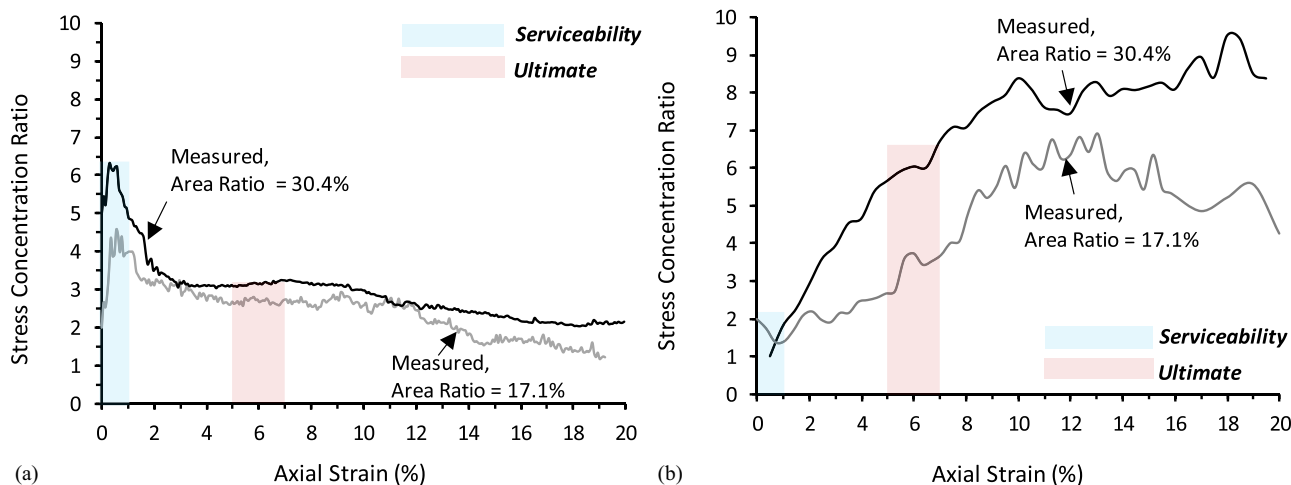


Fig. 16. Variation in the stress concentration ratio with axial strain for the drained and undrained tests: (a) CD-triaxial; and (b) CU-triaxial.

in sand compared with the stresses in sand observed in the control sand specimen that was sheared under true undrained conditions. This local partial drainage in the case of composite specimens is expected to prohibit the dense sand columns from generating negative pore-water pressure even under fast loading rates. Unlike the undrained control sand specimen that exhibited a maximum peak deviatoric stress of about 1,800 kPa [not shown in Fig. 15(d) so as not to distort the scale of the y -axis], the maximum stresses in sand in the sand columns did not exceed 210 kPa for the composite specimen with $a_r = 17.1\%$ and 375 kPa for specimens with $a_r = 30.4\%$. In fact, the stresses in the sand in the case of $a_r = 17.1\%$ (undrained test) were smaller than the stresses in sand observed in the identical drained test. The combination of low undrained shear strength in the surrounding clay and the inability to generate negative pore-water pressure in the columns due to partial drainage resulted in extremely small stresses in the sand in the undrained test involving an a_r of 17.1%.

Stress Concentration Ratio

The stress concentration ratio was calculated for all composite specimens by dividing the average measured stresses in sand (MP1 and MP2) by the stresses in clay measured with sensor MP3 at all strain levels, except for the undrained test under an a_r of 17.1%, where only the measured stress in sand from sensor MP1 was used in the analysis. The variation in the stress concentration ratio with axial strain is presented in Figs. 16(a and b) for the drained and undrained tests, respectively.

The results in Fig. 16 reveal a clear distinction between the mechanics of load sharing under both drained and undrained conditions. For the drained tests, the variation in the stress concentration ratio with strain shows a sharp increase in the ratio at relatively low strains, reaching maximum values of 4.5 and 6.3 for area replacement ratios of 17.1% and 30.4%, respectively. After the peak, the stress concentration ratio decreases gradually to reach values as low as 1.5 at large axial strains. Conversely, the variation in the stress concentration ratio with strain in undrained tests indicates a gradual monotonous increase, leading to peaks in the order of 6.5 and 9.5 for area replacement ratios of 17.1% and 30.4%, respectively. These peaks are observed at relatively large strains (greater than 13%). It should be noted that irrespective of the drainage conditions, the cases with the higher area replacement ratios resulted in the higher stress concentration ratios, which is in line with the work of Bachus and Barksdale (1984).

For the drained tests, the early peaks in the stress concentration ratio and the gradual but significant reduction that follows can be attributed to two main factors: (1) the softening that is observed in the sand columns that dilate and soften at relatively small strains; and (2) the progressive gradual strain hardening that is exhibited in the clay surrounding the columns as the clay consolidates and compresses during drained shear (Black et al. 2011). These two factors lead to an initial early peak in the stress concentration ratio followed by a significant reduction at large strains.

For the undrained tests, the monotonous increase in the stress concentration ratio with strain and the significantly larger stress concentration ratios in the specimens reinforced at the higher area replacement ratio of 30.4% can be attributed to two main factors: (1) the undrained conditions that governed the response of the clay in the composite specimens leading to the mobilization of relatively low undrained stresses in the clay, irrespective of the area replacement ratio [Fig. 15(b)]; and (2) the gradual increase in the mobilization of stresses in sand with strain (up to strains in the order of 10%) and the clear superior response of the 40 mm sand columns compared with the 30 mm columns [Fig. 15(d)]. The superior response of the sand columns in the specimen reinforced at an area replacement ratio of 30.4% is a direct consequence of the drainage conditions within the composite specimen and the role that the large diameter sand columns played in reducing the overall generation of positive pore-water pressure in the composite specimen.

The results in Fig. 16 point to several implications that could affect the design of clay systems that are reinforced with granular columns in practical field applications. The first implication is the importance of identifying the strain range that is relevant to practical design, given the significant variations that the stress concentration ratios exhibited in Fig. 16. For applications in which serviceability limit states are expected to govern the design of the reinforced clay system, the results in Fig. 16 indicate that stress concentration ratios in the range of 3–4 ($a_r = 17.1\%$) and 5–6 ($a_r = 30.4\%$) should be adopted in quantifying the load sharing between the clay and the sand column group if drained conditions are expected to govern. The stress concentration ratios pertain to estimated axial strains that are less than 1% in the shaded area in Fig. 16. If the designer is interested in the ultimate limit state (failure of the composite system), the strain range of interest shifts to around 5% to 7% (see Fig. 11). In this strain range, the stress concentration factors that should be adopted in design assuming

drained conditions reduce to around 2.5–3.0 (see the shaded area in Fig. 16).

If fast loading conditions that will result in an *undrained* response in the clay are expected to govern the design, the results in Fig. 16 indicate that for serviceability considerations, stress concentration factors as low as 1.5–2.0 are required to model the load sharing between the sand and the clay. For ultimate limit state considerations that involve undrained failure, stress concentration factors as high as 2.5–3.5 ($a_r = 17.1\%$) and 5.5–6.5 ($a_r = 30.4\%$) should be adopted to realistically model the stress distribution. It should be noted that these ranges for the stress concentration factor apply to the clay and sand used in this study and should not be generalized to cases involving different soil conditions.

Conclusions

In this paper, a newly developed fully instrumented large triaxial system is introduced to examine the behavior of soft clay specimens reinforced with group granular columns under both drained and undrained conditions. An innovative upper cap with three miniature pressure sensors and two pore-water pressure sensors was designed with proper calibration of the contact pressure sensors on different soil types and conditions.

Tests on large control clay specimens and specimens reinforced with a group of four sand columns at two area replacement ratios ($a_r = 17.1\%$ and 30.4%) were conducted under drained and undrained conditions. The stress measurements were used to investigate the mechanics of the stress distribution and load sharing between the sand column group and the surrounding clay, with emphasis on identifying the variation in the stress concentration ratios with strain and their dependence on the drainage conditions and area replacement ratio. Based on the results, the following conclusions can be made:

1. The newly developed instrumented large-scale triaxial setup allowed for collecting reliable data on pore pressures, volume change, overall deviatoric stress, and the development of local stresses in the clay and the surrounding columns. The measurements were repeatable and reliable for studying the mechanism of the interaction between the sand column group and the surrounding clay under different drainage conditions and rates of loading.
2. The use of dense sand columns to reinforce soft kaolin clay at area replacement ratios of 17.1% and 30.4% could increase the drained ultimate strength of the specimen by 8% and 40%, and the undrained strength by 39% and 159%, respectively. This increased strength is attributed to the dense columns' ability to carry additional stresses. This was proved by the miniature pressure sensors' measurements placed above dense sand columns that showed mobilized stresses as high as 350 kPa. In comparison, the miniature pressure sensors above the clay annulus indicated stresses as low as 50–60 kPa.
3. Local stress measurements indicated that the stress concentration ratios varied significantly with strain, rate of loading, and area replacement ratio. At very low axial strains and under drained conditions, stress concentration ratios between 4 and 6 could be mobilized. These relatively high ratios decrease to about 1.5 at relatively large strains. For the case of undrained loading, the stress concentration factors are very low (1.5–2) at small strains and increase to values as high as 6.5 and 9.5 for cases involving area replacement ratios of 17.1% and 30.4%, respectively.

Limitations of the Present Study and Scope for Future Work

It should be noted that the measured stress concentration factors pertain to the particular case of a clay specimen that is reinforced with a group of four sand columns. For a given area replacement ratio, there is a possibility that the measured stress concentration factor might be affected by the number and configuration of the columns in the group (triangular versus square configurations). Possible differences in the response for single and multiple column cases can be related to differences in the slenderness ratio of the columns (length to diameter ratio). In a triaxial setup, a single large-diameter central column will exhibit a smaller slenderness ratio than multiple columns do. In addition, clay specimens that are reinforced with a single column may exhibit an internal state of stress that may locally diverge from that exhibited in the multiple column case, where the shear plane will have to interact with multiple columns. Moreover, the stress state in the two cases might be affected by local differences in the internal drainage conditions and column stiffness. The effect of these parameters on the response of the composite and particularly on the stress concentration factors will be studied in future work.

The sand columns used in this research are of direct relevance to applications related to the use of granular columns as vertically draining elements (sand drains) or as reinforcing elements (sand compaction piles). As far as the comparison with stone or gravel columns and the potential size (or scale) effects, the use of sand columns instead of gravel or stone columns in physical modeling is dictated by testing constraints. The size of specimens that can be accommodated in triaxial setups is limited even in the large triaxial cell used in this study. Nevertheless, results from published studies indicate that the type of material used to construct the granular column (gravel, sand, or a mixture of both) does not change the mechanics of the interaction between the columns and the surrounding clay. The reported stress concentration ratios in this study are very much needed for a better understanding of the load-transfer mechanism between the clay matrix and the granular columns in applications involving both short and long-term stability of foundations.

Data Availability Statement

All data, models, and code generated or used during the study appear in the published article.

Acknowledgments

The authors acknowledge the support of the University Research Board (URB) at the American University of Beirut for funding this research program.

References

- AlMikati, A., S. Najjar, and S. Sadek. 2020. "The drained response of soft clays reinforced with sand column groups." In *Geo-Congress 2020: Foundations, Soil Improvement, and Erosion*, 411–420. Reston, VA: ASCE.
- Andreou, P., W. Frikha, R. Frank, J. Canou, V. Papadopoulos, and J. C. Dupla. 2008. "Experimental study on sand and gravel columns in clay." *Proc. Inst. Civ. Eng. Ground Improv.* 161 (4): 189–198. <https://doi.org/10.1680/grim.2008.161.4.189>.

- Aslani, M., J. Nazariafshar, and N. Ganjian. 2019. "Experimental study on shear strength of cohesive soils reinforced with stone columns." *Geotech. Geol. Eng.* 37 (3): 2165–2188. <https://doi.org/10.1007/s10706-018-0752-z>.
- ASTM. 2011. *Standard test method for consolidated drained triaxial compression test for soils*. D7181. Reston, VA: ASTM.
- Bachus, R. C., and R. D. Barksdale. 1984. "Vertical and lateral behavior of model stone columns." In *Proc. Int. Conf. on In Situ Soil and Rock Reinforcement*, 99–104. Paris: Colloque International.
- Baumann, V., and G. E. A. Bauer. 1974. "The performance of foundations on various soils stabilized by the vibro-compaction method." *Can. Geotech. J.* 11 (4): 509–530. <https://doi.org/10.1139/t74-056>.
- Black, J., V. Sivakumar, M. R. Madhav, and B. McCabe. 2006. "An improved experimental test set-up to study the performance of granular columns." *Geotech. Test. J.* 29 (3): 193–199.
- Black, J., V. Sivakumar, and J. D. McKinley. 2007. "Performance of clay samples reinforced with vertical granular columns." *Can. Geotech. J.* 44 (1): 89–95. <https://doi.org/10.1139/t06-081>.
- Black, J. A., V. Sivakumar, and A. Bell. 2011. "The settlement performance of stone column foundations." *Géotechnique* 61 (11): 909–922. <https://doi.org/10.1680/geot.9.P.014>.
- Casagrande, A. 1936. "The determination of pre-consolidation load and its practical significance." In Vol. 3 of *Proc. Int. Conf. Soil Mechanics and Foundation Engineering*, 60. Cambridge, MA: Harvard University.
- Charles, J. A., and K. A. Watts. 1983. "Compressibility of soft clay reinforced with granular columns." In *Proc., 8th European Conf. on Soil Mechanics and Foundation Engineering*, 347–352. Rotterdam, The Netherlands: AA Balkema.
- Cimentada, A., A. Da Costa, J. Cañizal, and C. Sagaseta. 2011. "Laboratory study on radial consolidation and deformation in clay reinforced with stone columns." *Can. Geotech. J.* 48 (1): 36–52. <https://doi.org/10.1139/T10-043>.
- Fattah, M. Y., K. T. Shlash, and M. J. M. Al-Waily. 2011. "Stress concentration ratio of model stone columns in soft clays." *Geotech. Test. J.* 34 (1): 50–60.
- Ghazavi, M., and J. N. Afshar. 2013. "Bearing capacity of geosynthetic encased stone columns." *Geotext. Geomembr.* 38: 26–36. <https://doi.org/10.1016/j.geotexmem.2013.04.003>.
- Hu, W. 1995. "Physical modelling of group behaviour of stone column foundations." Ph.D. thesis, Dept. of Infrastructure and Environmental Engineering, Univ. of Glasgow.
- Hugher, J. M. O., and N. J. Withers. 1974. "Reinforcing of soft cohesive soils with stone columns." *Ground Eng.* 7 (3): 42–49.
- Juran, I., and A. Guermazi. 1988. "Settlement response of soft soils reinforced by compacted sand columns." *J. Geotech. Eng.* 114 (8): 930–943. [https://doi.org/10.1061/\(ASCE\)0733-9410\(1988\)114:8\(930\)](https://doi.org/10.1061/(ASCE)0733-9410(1988)114:8(930)).
- Kim, D., and J. R. Kim. 2007. "Resilient behavior of compacted subgrade soils under the repeated triaxial test." *Constr. Build. Mater.* 21 (7): 1470–1479. <https://doi.org/10.1016/j.conbuildmat.2006.07.006>.
- Lin, H., and D. Penumadu. 2005. "Experimental investigation on principal stress rotation in Kaolin clay." *J. Geotech. Geoenviron. Eng.* 131 (5): 633–642. [https://doi.org/10.1061/\(ASCE\)1090-0241\(2005\)131:5\(633\)](https://doi.org/10.1061/(ASCE)1090-0241(2005)131:5(633)).
- McCabe, B. A., and M. M. Killeen. 2017. "Small stone-column groups: Mechanisms of deformation at serviceability limit state." *Int. J. Geomech.* 17 (5): 04016114. [https://doi.org/10.1061/\(ASCE\)GM.1943-5622.0000700](https://doi.org/10.1061/(ASCE)GM.1943-5622.0000700).
- McKelvey, D., V. Sivakumar, A. Bell, and J. Graham. 2004. "Modelling vibrated stone columns in soft clay." *Proc. Inst. Civ. Eng. Geotech. Eng.* 157 (3): 137–149. <https://doi.org/10.1680/geng.2004.157.3.137>.
- Miranda, M., A. Da Costa, J. Castro, and C. Sagaseta. 2017. "Influence of geotextile encasement on the behaviour of stone columns: Laboratory study." *Geotext. Geomembr.* 45 (1): 14–22. <https://doi.org/10.1016/j.geotexmem.2016.08.004>.
- Murugesan, S., and K. Rajagopal. 2010. "Studies on the behavior of single and group of geosynthetic encased stone columns." *J. Geotech. Geoenviron. Eng.* 136 (1): 129–139. [https://doi.org/10.1061/\(ASCE\)GT.1943-5606.0000187](https://doi.org/10.1061/(ASCE)GT.1943-5606.0000187).
- Najjar, S. S. 2013. "A state-of-the-art review of stone/sand-column reinforced clay systems." *Geotech. Geol. Eng.* 31 (2): 355–386. <https://doi.org/10.1007/s10706-012-9603-5>.
- Najjar, S. S., S. Sadek, H. Bou Lattouf, and Y. Maalouf. 2020. "Drained triaxial response of clay reinforced with sand columns." *Proc. Inst. Civ. Eng. Ground Improv.* 173 (3): 170–186. <https://doi.org/10.1680/jgrim.18.00007>.
- Najjar, S. S., S. Sadek, and T. Maakaroun. 2010. "Effect of sand columns on the undrained load response of soft clays." *J. Geotech. Geoenviron. Eng.* 136 (9): 1263–1277. [https://doi.org/10.1061/\(ASCE\)GT.1943-5606.0000328](https://doi.org/10.1061/(ASCE)GT.1943-5606.0000328).
- Nazariafshar, J., N. Mehrannia, F. Kalantary, and N. Ganjian. 2019. "Bearing capacity of group of stone columns with granular blankets." *Int. J. Civ. Eng.* 17 (2): 253–263. <https://doi.org/10.1007/s40999-017-0271-y>.
- Sivakumar, V., D. K. N. M. Jeludine, A. Bell, D. T. Glynn, and P. Mackinnon. 2011. "The pressure distribution along stone columns in soft clay under consolidation and foundation loading." *Géotechnique* 61 (7): 613–620. <https://doi.org/10.1680/geot.9.P.086>.
- Sivakumar, V., D. McKelvey, J. Graham, and D. Hughes. 2004. "Triaxial tests on model sand columns in clay." *Can. Geotech. J.* 41 (2): 299–312. <https://doi.org/10.1139/t03-097>.
- Sivakumar, V., D. McKelvey, D. Hughes, and J. Graham. 2003. "Clay reinforcement using sand columns: performance under triaxial loading." *Can. Geotech. J.* 41 (2): 299–312. <https://doi.org/10.1139/t03-097>.
- Skempton, A. W. 1954. "The pore-pressure coefficients A and B." *Géotechnique* 4 (4): 143–147. <https://doi.org/10.1680/geot.1954.4.4.143>.
- Stuedlein, A. W., and R. D. Holtz. 2012. "Analysis of footing load tests on aggregate pier reinforced clay." *J. Geotech. Geoenviron. Eng.* 138 (9): 1091–1103. [https://doi.org/10.1061/\(ASCE\)GT.1943-5606.0000677](https://doi.org/10.1061/(ASCE)GT.1943-5606.0000677).
- White, D. J., H. T. Pham, and K. K. Hoevelkamp. 2007. "Support mechanisms of rammed aggregate piers. I: Experimental results." *J. Geotech. Geoenviron. Eng.* 133 (12): 1503–1511. [https://doi.org/10.1061/\(ASCE\)1090-0241\(2007\)133:12\(1503\)](https://doi.org/10.1061/(ASCE)1090-0241(2007)133:12(1503)).
- Wood, M., W. Hu, and D. F. Nash. 2000. "Group effects in stone column foundations: Model tests." *Géotechnique* 50 (6): 689–698. <https://doi.org/10.1680/geot.2000.50.6.689>.